Cyclotron resonance and cyclotron waves at far-infrared frequencies in a semimetal with nonparabolic bands

A. Miklavc*†
Boris Kidrič Institute of Chemistry, 61000 Ljubljana, Yugoslavia

H. D. Drew
Department of Physics and Astronomy, University of Maryland, College Park, Maryland 20742
(Received 29 August 1977; revised manuscript received 7 October 1980)

We develop a theory of quantum cyclotron resonance in semimetals at far-infrared frequencies, assuming the ordinary polarization ($E \| H_0$) and the ellipsoidal nonparabolic two-band model, and compare it with the second harmonic, measured for the same polarization in bismuth at 890.7 and 964.3 GHz. For this purpose we derive the corresponding nonlocal conductivity tensor in a way which takes the nonparabolicity fully into account and which enables us to relate lifetimes to quantities calculable microscopically. Although the theory derived is not exact, it accounts in a quantitative way for the important features of the observed spectra. We show that absorption on the high-field side of the resonances is related to high-frequency cyclotron waves propagating in the sample, which are damped and have reduced amplitudes due to the finite lifetimes and due to the electrons which collide with the surface and are thus nonresonant. It was therefore necessary to find an adequate treatment of the surface effects. The only adjustable parameters in the theory are the band parameters and lifetimes. To get a good agreement with the experiment it was necessary to assume that the lifetimes were energy dependent. We made only a very approximate estimate of this dependence. A more careful study of the lifetimes is left for a subsequent paper.

I. INTRODUCTION

Cyclotron resonance is presently one of the main methods of investigating the properties of the electric carriers in solids. The resonance has its origin in resonant absorption of the incident high-frequency electromagnetic radiation by the carriers, circulating about the applied static magnetic field H_0 with the cyclotron frequency ω_c. The observed spectra of the resonance, however, depend rather drastically on which system we are looking at and are sometimes difficult to interpret.[1,2] For instance, cyclotron resonance in lightly doped semiconductors may or may not occur at the cyclotron frequency ω_c, depending on whether or not the frequency of the incident radiation ω is much greater than or less than the plasma frequency ω_p. In metals or in semimetals, where $\omega_p \gg \omega$, one usually observes a series of resonances periodic in $1/H_0$, where H_0 is the applied magnetic field. Each resonance occurs at $\omega = n\omega_c$, where n is an integer. In the vicinity of the resonance the dielectric constant of the carriers becomes real and positive so that magnetoplasma waves[1,2] may propagate in the sample. Their behavior depends strongly on the shape of Fermi surface, on the direction of magnetic field, and on the density of the carriers and their lifetimes. In addition, the presence of the surface can affect excitation of these waves rather strongly. To predict the line shapes and relative intensities of the experimentally observed peaks is therefore a difficult boundary-value problem and until now it has only been solved by some approximate methods. The kind of assumptions one makes in these approximations depends again on the properties of the particular system we are looking at.

Classically speaking, electrons in a magnetic field describe helical paths about the magnetic field vector. The gyration of electrons is characterized by the cyclotron frequency $\omega_c = eH_0/mc$ and by the cyclotron radius $R_c \sim v_F/\omega_c$, where $v_F \sim 10^8$ cm s^{-1} is the Fermi velocity. An important parameter is electron lifetime τ. The electromagnetic properties at low frequencies, i.e., when $\omega\tau \ll 1$, differ in most cases from those at high frequencies, characterized by $\omega\tau \gg 1$. When $\omega_c\tau \gg 1$ and $\omega \lesssim \omega_c$ an electron makes at least one complete revolution during the electromagnetic field period, and the action of magnetic field is manifested most distinctly. The cyclotron wave spectrum arising in strong magnetic fields therefore usually terminates at frequencies higher than the cyclotron frequency ω_c. If the variation of the high-frequency ($\omega\tau \gg 1$) electromagnetic field over the effective range $l^* = v/\omega$ of the carrier (i.e., the distance traversed by the carrier in one period of the electric field) is small, then the nonlocal effects do not play any role and the skin effect is normal.

(This is true whatever the value of the mean free path $l = \tau v_F$.) In the absence of a constant magnetic field, the dielectric constant of metals and semimetals is negative and the field actually attenuates exponentially over a distance $\sim\delta_0 = c/\omega_p$ from the surface, δ_0 being usually called the skin depth. The condition of the normal skin effect at $H_0 = 0$ is thus given by $l^* \ll \delta_0$. In the regime of cyclotron resonance, where $\omega \sim \omega_c$, the effective range l^* is of the order of the cyclotron radius R_c. It can therefore be assumed that in the limit $R_c \ll \delta_0$ the spatial inhomogeneity of the high-frequency electric field over the trajectory of a carrier is small, and consequently, local theory is applicable.

In metals, we have $R_c > \delta_0$ and therefore nonlocal theory is needed. There exists no exact solution[3] of the electrodynamics in metal when magnetic field is parallel to its surface, even for the simplest case of a spherical Fermi surface. Approximate solutions have been obtained, however, in a number of physically interesting situations,[4–8] starting with the most noteworthy original work of Azbel' and Kaner[4] on cyclotron resonance in metals. These theories can explain reasonably well the cyclotron resonance in metals at microwave and also at far-infrared frequencies.

In bismuth, the plasma frequency is smaller by more than one order of magnitude than in typical metals. Accordingly, the characteristic distance over which electromagnetic field changes appreciably is much larger than in metals, and the cyclotron radius becomes smaller than the skin depth, $R_c < \delta_0$, at least at the far-infrared frequencies. Cyclotron resonance in bismuth under local conditions was investigated by Smith, Hebel, and Buchsbaum.[9] They concluded that in the local limit cyclotron resonance of one definite group of carriers is impossible. The resonance is screened by a longitudinal depolarizing field[10] which couples strongly the longitudinal and transverse degrees of freedom of the plasma and shifts the resonant frequencies away from the cyclotron frequencies of electrons and holes. The resonant frequencies are hybrid[9] and include the cyclotron masses of all the carrier groups. Cyclotron resonance is possible only at such directions of the magnetic field for which the cyclotron masses of two nonequivalent electron groups are the same but their orbits are inclined at different angles to the magnetic field. Such a resonance is called "tilted orbit cyclotron resonance."

Actually, besides the hybrid resonances and resonances on tilted orbits, the experimental curves in Ref. 9 reveal the presence of maxima corresponding to cyclotron resonance of an individual carrier group. This fact offers evidence of the nonapplicability of the local theory to the analysis of cyclotron resonance in bismuth. Subsequently Hebel[11] has shown that a small but finite spatial inhomogeneity of the field gives rise to a resonant term in the dielectric constant and in the absorption coefficient. Hebel considered cyclotron resonance of holes for the polarization of the electric field E along the constant magnetic field H_0 ("ordinary wave") and confined himself to the case of $R_c \ll \delta_0$ when the resonant part of the dielectric constant due to the nonlocal effect is a small resonant addition to the main local term. In this case the propagation of the cyclotron wave is still impossible since the dielectric constant remains negative. Brovtsyna and Skobov[12] made a more complete study of the nonlocal effects on the cyclotron resonance of holes in the regime $R_c/\delta_0 \ll 1$ and discussed the conditions under which one can expect that a weakly damped cyclotron wave would exist in the sample. They demonstrated that an allowance for cyclotron waves is essential in studies of the line shape of cyclotron resonance in bismuth. This conclusion is supported by the results of the work, both experimental and theoretical, on the spectra of these waves, associated with the cyclotron resonance of electrons in bismuth at frequencies around 10 GHz, which were reported by Edel'man.[13]

The investigations mentioned so far are all classical in nature, that is, quantum theory is not needed to understand the experimental results. (The photon energy $\hbar\omega$ and thermal energy kT at temperatures $\sim$4 K are very much less than Fermi energy E_F.) Fairly recently the cyclotron resonance experiments in bismuth have been reported[14,15] at the far-infrared laser frequencies around 1000 GHz. In these experiments distinct quantum transitions were presumably observed between a pair of Landau levels in the nonparabolic conduction band of bismuth. Because of the nonparabolicity, the subharmonics are split, the nth subharmonic consisting of n peaks, each being assigned to a distinct quantum transition. The far-infrared frequencies of these experiments are also significant in that they are comparable to zone-boundary acoustic- and optical-phonon frequencies in bismuth. One might expect that some effects of the electron-phonon interaction could be observed in the form of an energy-dependent cyclotron mass, or an energy-dependent cyclotron mass, or an energy-dependent electronic lifetime, similar to those found in metals.[16] Because of lack of a satisfactory theory of the cyclotron resonance line shape neither the resonance position nor the electronic lifetime have been determined to the accuracy warranted by the accuracy of the experiments. This is particularly true for the lifetimes.

It is the purpose of the present work to investigate the line shape of the cyclotron resonance in bismuth in the regime in which the above-mentioned experiments were carried through ($\omega\tau \gg 1$, $R_c < \delta_0$) so that one could extract the information on bismuth band parameters and lifetimes from the available data. We also hope to elucidate more general features of the quantum cyclotron resonance in this

regime when bands are nonparabolic and nonlocal effects are important and, in addition, the effects of the surface scattering cannot be neglected. The acquired knowledge could, hopefully, be used to understand data from other materials (semimetals, degenerate semiconductors) where the resonance can be observed under the conditions similar to those in bismuth at far-infrared frequencies.

We shall concentrate our efforts on the second harmonics. The main reason for this is that the experimental technique that was used in obtaining these spectra did not give reliable results for the case of large signals so that the observed line shape of the first harmonics could not be trusted.[17] Experimental data were obtained with E both perpendicular and parallel to H_0, and for several orientations of the crystal. In geometries with $E \perp H_0$ one must take into account the Hall fields which makes the calculations become exceedingly cumbersome. We shall therefore limit our study to the cases where $E \parallel H_0 \parallel$ binary axis, with surface of the sample perpendicular to the bisectrix axis. There is no Hall effect in this geometry and, by making this choice, we do not lose any of the important features of the resonance.

II. BAND STRUCTURE

Before proceeding with our discussion of cyclotron resonance, we need to describe briefly the nonparabolic band structure, as it is found in bismuth. It is presently quite firmly established, except for a few details. (For a recent review see the work of McClure.[18]) The three mutually perpendicular crystal axis of bismuth, i.e., the binary, the bisectrix, and the trigonal axis, will be labeled by x, z, and y throughout this entire work.

A large part of experimental observations in bismuth can be explained on the basis of the two-band model, proposed by Lax and Mavroides.[19] The model is based upon the fact that at the L point in the Brillouin zone, where the electron pockets in bismuth are located, the conduction and the valence band are separated only by a small energy gap of ~ 0.01 eV, and the other bands are at least an order of magnitude further away. The dispersion relation in the two-band model in which these other bands are neglected can be obtained from $\vec{k} \cdot \vec{p}$ perturbation theory and is given by

$$E^{(\pm)}(\vec{k}) = -\tfrac{1}{2}E_g \pm \tfrac{1}{2}\left[E_g^2 + 2E_g\hbar^2 \frac{\vec{k}\cdot\vec{\alpha}^*\cdot\vec{k}}{m}\right]^{1/2} . \quad (2.1)$$

(+) and (−) refer to the conduction and the valence bands, respectively. E_g is the gap energy separating the two bands and m is the electron rest mass. $\vec{\vec{\alpha}}^*$ is a dimensionless inverse effective mass tensor which refers to curvatures of the bottom of the conduction band. It is of the form

$$\vec{\vec{\alpha}}^* = \begin{pmatrix} \alpha_{xx}^* & 0 & 0 \\ 0 & \alpha_{zz}^* & \alpha_{zy}^* \\ 0 & \alpha_{zy}^* & \alpha_{yy}^* \end{pmatrix} . \quad (2.2)$$

The inverse mass tensor at the Fermi surface $\vec{\vec{\alpha}}$ can be expressed in terms of that at the band minimum $\vec{\vec{\alpha}}^*$ by the relation

$$\vec{\vec{\alpha}}(E_F) \equiv \vec{\vec{\alpha}} = \left[\frac{E_g}{E_g + 2E_F}\right]\vec{\vec{\alpha}}^* . \quad (2.3)$$

The two-band model thus gives a nonparabolic dispersion relation, however constant energy surfaces are ellipsoidal. For this reason it is often referred to as an ellipsoidal nonparabolic model. The electron Fermi surfaces are very elongated ellipsoids (ratio of the longitudinal to transversal mass is ~ 15) centered at the L points of the Brillouin zone (ellipsoids a, b, and c on Fig. 1). The ellipsoid a has its long axis almost parallel to the bisectrix direction. There is a $\sim 6°$ tilt of its long axis toward the trigonal direction which we will neglect in our considerations. The other two ellipsoids b and c can be obtained by rotating the ellipsoid a through $\pm 120°$ about the trigonal axis. The hole Fermi surface h, containing three times as many carriers as one electron ellipsoid, is at the T point. It is of very nearly ellipsoidal form and parabolic.

The energy levels in the presence of an external magnetic field H_0 are labeled by the orbital quantum number $n = 1, 2, 3, \ldots$, the spin quantum number $s = \pm\frac{1}{2}$ and the momentum k_H along the magnetic field H_0. As shown by Cohen and Blount,[20] the spin mass is equal to the cyclotron mass in the two-band model so that the levels have characteristic degeneracy

$$E(n+1, s=-\tfrac{1}{2}) = E(n, s=+\tfrac{1}{2}) . \quad (2.4)$$

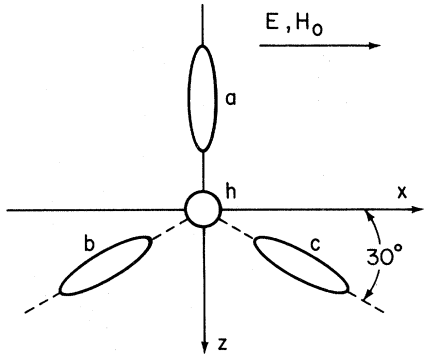

FIG. 1. Orientation of the Fermi surface of bismuth with respect to the applied fields and chosen coordinate system in the experiments for which our calculations were carried through. The Fermi-surface ellipsoids are not drawn in realistic proportions.

If we introduce the magnetic level index j

$$j = n + \tfrac{1}{2} - s, \quad n = 0, 1, 2, \ldots, \quad s = \pm\tfrac{1}{2} \tag{2.5}$$

we can then write the magnetic energy levels in the form

$$E_j^{(\pm)}(k_H) = -\tfrac{1}{2}E_g \pm \left[\tfrac{1}{4}E_g^2 + E_g\left(j\frac{e\hbar H_0}{m_c^* c} + \frac{\hbar^2 k_H^2}{2m_H^*}\right)\right]^{1/2} . \tag{2.6}$$

m_c^* and m_H^* are the cyclotron and longitudinal effective-mass values at the bottom of the nonparabolic band. They are related to the effective-mass tensor $\overline{\overline{m}}^* = (\overline{\overline{\alpha}}^*)^{-1}$ as follows:

$$m_H^* = \hat{h}\cdot\overline{\overline{m}}^*\cdot\hat{h}, \quad m_c^* = \left|\frac{\det\overline{\overline{m}}^*}{m_H^*}\right|^{1/2} , \tag{2.7}$$

where $\hat{h}$ is the unit vector in the direction of the magnetic field. Except for $j = 0$ the levels are doubly degenerate. Figure 2 represents the level structure for $H_0 \sim 5$ kG parallel to the binary axis.

The wave functions in the two-band model, in the case of an external magnetic field, were derived by Wolff.[21] He also obtained the matrix elements of the velocity operator

$$\vec{v}_{op} = \vec{\nabla}_k \hat{\mathcal{H}} , \tag{2.8}$$

which are of great importance since they determine the conductivity. He found that the velocity matrix element for the two-band model can be expressed in terms of matrix elements with respect to eigenfunctions of the effective-mass Hamiltonian $\hat{\mathcal{H}}^*$ [see Eq. (2.10) below]

$$\langle\psi|\vec{v}_{op}|\psi'\rangle = \left[E_g[E'E(2E+E_g)(2E'+E_g)]^{-1/2} \times\langle\chi|\left(\frac{\overline{\overline{\alpha}}^*\cdot\vec{\pi}}{2}(E+E'+E_g) + \frac{ic}{e}(\vec{\pi}\times\vec{\mu})(E-E')\right)|\chi'\rangle\right] . \tag{2.9}$$

Here E and E' are the energies [given by Eq. (2.6)] of the states $|\psi\rangle$ and $|\psi'\rangle$, each of which may be in either the conduction or valence bands; $|\chi\rangle$ and $|\chi'\rangle$ are the corresponding eigenstates of the effective-mass Hamiltonian $\hat{\mathcal{H}}^*$

$$\hat{\mathcal{H}}^* = \frac{\vec{\pi}\cdot\overline{\overline{\alpha}}^*\cdot\vec{\pi}}{2} - \vec{\mu}\cdot\vec{H}_0 , \tag{2.10}$$

$\vec{\mu}$ is the electron magnetic moment and $\vec{\pi} = \vec{p} - (e/c)\vec{A}$, where $\vec{A}$ is the vector potential of the external magnetic field.

Wolff also estimated[21] that the effective spin-resonance matrix element (M_{spin}) for intraband transitions is smaller than that for the cyclotron resonance ($M_{cyclotron}$) by about the ratio

$$\frac{\langle|M_{spin}|^2\rangle}{\langle|M_{cyclotron}|^2\rangle} \sim \left(\frac{\hbar\omega_c}{2(E_F+E_g)}\right)^2 . \tag{2.11}$$

In applying the two-band model to bismuth, it should be kept in mind that it is, at best, an approximation to the band structure. Cohen[22] pointed out that the experimentally observed values of $\overline{\overline{\alpha}}^*$ require the energy to be parabolic along the axis z. To eliminate this inconsistency he then proposed a new model with nonparabolic dispersion relation and nonellipsoidal constant-energy surfaces (NENP model). At present, the experimental evidence seems to be inconclusive with regard to validity of the NENP model. Careful experiments[23] sensitive to the shape of the Fermi surface in bismuth show a nearly ellipsoidal constant-energy surface, and hence there seems to be little necessity for choosing the Cohen's NENP model over the simpler ellipsoidal nonparabolic two-band model. In particular the low-mass directions should be well described by the two-band model.

The quantum oscillation experiments[24–29] revealed that the degeneracy of levels in bismuth is only approximate, with fractional deviation $\delta(n)$

$$\delta(n) = \frac{E(n+1, s=-\tfrac{1}{2}) - E(n, s=+\tfrac{1}{2})}{E(n+1, s=-\tfrac{1}{2}) - E(n, s=-\tfrac{1}{2})} \tag{2.12}$$

ranging from about 10 to 30%, depending on the direction of magnetic field. (It is about 10% in the binary direction.) The nonzero values for $\delta(n)$ arise from the presence of bands other than the two con-

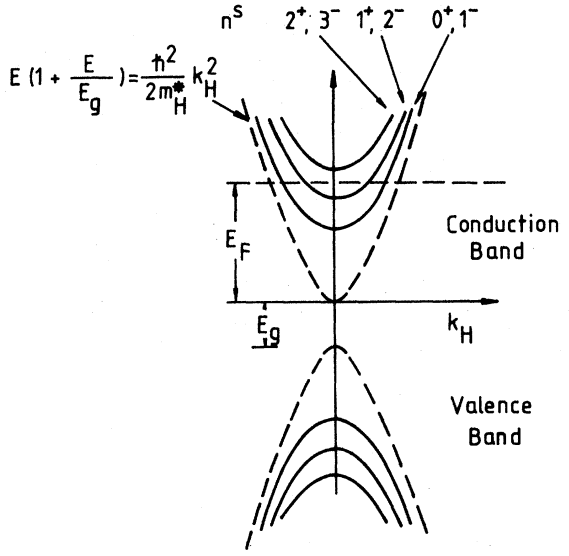

FIG. 2. Energy levels E_n of bismuth in the nonparabolic two-band model for magnetic field H_0 oriented along the binary axis. The field strength is 5 kG.

sidered in the two-band model. Corrections to the two-band model where studied by Baraff[30] and later also by a number of other authors (see Refs. 18 and 31 and the works cited therein).

We shall assume that the ellipsoidal nonparabolic two-band model is adequate to study the main features of the cyclotron resonance in our regime. A more accurate study of lifetime may require that we take spin splitting properly into account because nondegenerate spin levels could give rise to a broadening of cyclotron resonance lines. In this case one would then have to include also corrections to the two-band model mentioned above. This can be done without serious difficulty, however, at a price of a very complicated algebra.

III. ELECTRODYNAMICS OF METALS AND SEMIMETALS IN A HIGH-FREQUENCY ELECTROMAGNETIC FIELD

The behavior of a metal or a semimetal in a high-frequency electromagnetic field is described completely by its surface impedance $Z(\omega)$

$$Z=\frac{4\pi}{c}\frac{\mathcal{E}_t(0)}{H_t(0)}=\frac{4\pi i\omega\mu}{c^2}\left[\frac{\mathcal{E}_t}{\partial\mathcal{E}_t/\partial z}\right]_{+0} . \tag{3.1}$$

The index t denotes components of the field parallel to the surface of the sample. z is normal to the surface and directed inward. Sample fills the $z>0$ half-space and the wave is incident normal to its surface with $\vec{\mathcal{E}}$ and $\vec{H}_0$ both oriented along the x axis (Fig. 3).

The real part of the surface impedance Z (the surface resistance R) determines the energy loss of an electromagnetic wave upon reflection. It can be calculated once the electric field inside the sample is known. The field is determined by the pair of Maxwell equations

$$\mathrm{rot}\,\vec{\mathcal{E}}(\vec{x},t)=-\frac{1}{c}\frac{\partial}{\partial t}\vec{H}(\vec{x},t) , \tag{3.2a}$$

$$\mathrm{rot}\,\vec{H}(\vec{x},t)=\frac{4\pi}{c}\vec{j}(\vec{x},t)+\frac{\epsilon_0}{c}\frac{\partial}{\partial t}\vec{\mathcal{E}}(\vec{x},t) , \tag{3.2b}$$

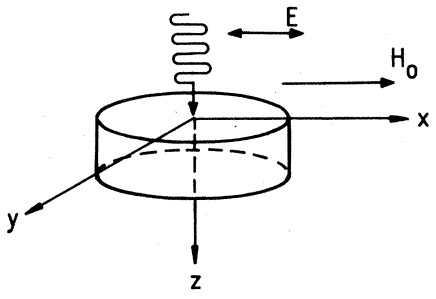

FIG. 3. Specification of coordinate axes relative to the sample surface and applied fields.

where $\vec{j}(\vec{x},t)$ is the conduction current density and ϵ_0 is the dielectric constant of the lattice. The second term on the right-hand side of Eq. (3.2b) comes from the displacement current. This term is negligibly small in metals at microwave frequencies. In bismuth, however, $\epsilon_0\simeq 100$ and $\omega_p\simeq 3\times 10^{14}$ Hz so that the displacement current may not be negligible when working with far-infrared frequencies.

For mathematical convenience, we will imagine that the $z<0$ half-space is filled with the image metal and that the fields and currents in both half-spaces are induced by a current sheet $2I_s\delta(z)$ at $z=0$ which has the strength $2I_s$ per unit width. By symmetry, this sheet induces mirror-symmetric electron current distribution in the real metal and the image metal, with $J(z)=J(-z)$ and correspondingly $\mathcal{E}(z)=\mathcal{E}(-z)$. Since the fields and currents fall to zero at $|z|\to\infty$, the total electron current must exactly screen the source current in the sheet, so that

$$I_s=-\int_0^\infty J(z)\,dz=\frac{c^2\mathcal{E}'(+0)}{4\pi i\omega} , \tag{3.3}$$

where $\mathcal{E}'(+0)=d\mathcal{E}(z)/dz|_{z\to+0}$. We emphasize that the plane $z=0$ forms a genuine boundary between the two half-spaces, so that electrons approaching it from either side are reflected back instead of crossing it.

In bismuth, at frequencies $\sim$900 GHz, we find that, at the cyclotron resonance, the ratio of cyclotron radius to skin depth is $R_c/\delta_0\sim\frac{1}{3}$. Therefore, according to what is said in the Introduction, the relation between field and current is nonlocal

$$j_i(\vec{x})=\int d^3x'\,\sigma_{ik}(\vec{x},\vec{x}')\mathcal{E}_k(\vec{x}') . \tag{3.4}$$

Because of surface effects the tensor $\sigma_{ik}(\vec{x},\vec{x}')$ does not depend on the difference $\vec{x}-\vec{x}'$ only, as it would for an unbounded medium. It is clear, on physical grounds, that sufficiently far from the surface its effects on the conductivity vanish so that the conductivity becomes equal to that of the continuum. Therefore it is convenient to write the total conductivity tensor as a sum

$$\sigma_{ik}(\vec{x},\vec{x}')=\sigma_{ik}^{\infty}(\vec{x},\vec{x}')+\sigma_{ik}^{s}(\vec{x},\vec{x}') , \tag{3.5}$$

where $\sigma_{ik}^{\infty}(\vec{x},\vec{x}')$ is the bulk conductivity (and thus depends on $\vec{x}-\vec{x}'$ only) and $\sigma_{ik}^{s}(\vec{x},\vec{x}')$ is due to the surface effects. The expressions for both σ_{ik}^{∞} and σ_{ik}^{s} will be derived in Secs. IV–VI. The general form of σ_{ik}^{∞} depends on the geometry of experiment. In our case both, the incident $\vec{\mathcal{E}}$ field and the constant $\vec{H}_0$ field are along the binary axis (x axis, see, Fig. 1) i.e.,

$$\vec{\mathcal{E}}=(\mathcal{E},0,0),\quad \vec{H}_0=(H_0,0,0) , \tag{3.6}$$

and the tensor σ_{ik}^{∞} is of the form[32]

$$\sigma_{ik}^{\infty}=\begin{pmatrix}\sigma_{xx}^{\infty} & 0 & 0\\ 0 & \sigma_{zz}^{\infty} & \sigma_{zy}^{\infty}\\ 0 & \sigma_{yz}^{\infty} & \sigma_{yy}^{\infty}\end{pmatrix} . \tag{3.7}$$

Let us for a moment neglect all surface effects. The Maxwell equations (3.2) then lead to the following system of equations for the Fourier components $E_i(q)$ of the electric field in the sample

$$\vec{q}(\vec{q}\cdot\vec{E})-q^2\vec{E}+k_0^2\vec{\epsilon}\cdot\vec{E}=0 , \tag{3.8}$$

where $k_0=\omega/c$ and

$$\epsilon_{\alpha\beta}(\vec{q},\omega,\vec{H}_0)=\epsilon_0\delta_{\alpha\beta}+\frac{4\pi i}{\omega}\sigma_{\alpha\beta}^{\infty}(\vec{q},\omega,\vec{H}_0) \tag{3.9}$$

is the dielectric tensor of the bulk. Since in our case $\vec{q}=(0,q,0)$ the system (3.8) can also be written

$$\begin{aligned}&(k_0^2\epsilon_{xx}-q^2)E_x=0 ,\\ &\epsilon_{zz}E_z+\epsilon_{zy}E_y=0 ,\\ &k_0^2\epsilon_{yz}E_z+(k_0^2\epsilon_{yy}-q^2)E_y=0 .\end{aligned} \tag{3.10}$$

The determinant of the system (3.10) must be equal to zero for a nontrivial solution $\vec{E}(q)$ to exist. This condition leads us to the equation

$$\left(\frac{q^2}{k_0^2}-\epsilon_{xx}\right)\left(\frac{q^2}{k_0^2}-\epsilon_{yy}+\frac{\epsilon_{zy}\epsilon_{yz}}{\epsilon_{zz}}\right)=0 \tag{3.11}$$

the roots of which are the possible wave vectors in the unbounded solid. When the first factor in Eq. (3.11) is zero, the electric field is of the form $\vec{E}=(E_x,0,0)$ and ϵ_{xx} alone determines the dispersion relation. This is the case in our geometry. The second possible solution of Eq. (3.10) is of the form $\vec{E}=(0,E_z,E_y)$ and corresponds to the second factor in Eq. (3.11) being equal to zero. This situation is realized in experiments where $\vec{E}\perp\vec{H}_0$. In this case the longitudinal component of electric field is in general not equal to zero, because of the Hall effect.

We shall assume that the tensor σ_{ik}^{s} is of the same form as σ_{ik}^{∞} [see Eq. (3.7)] and that the presence of the surface does not change the character of the field inside the sample so that the total current density has x component only

$$\vec{j}=(j,0,0) . \tag{3.12}$$

Equations (3.2)–(3.7) and (3.12) can be combined to give

$$\frac{d^2}{dz^2}\mathcal{E}(z)+\epsilon_0\frac{\omega^2}{c^2}\mathcal{E}(z)=-\frac{4\pi i\omega}{c^2}j+2\mathcal{E}'(+0)\delta(z) . \tag{3.13}$$

We express each term as a Fourier integral and find, using Eqs. (3.4) and (3.5), and putting $E\equiv E_x$

$$\left(-q^2+\frac{\omega^2}{c^2}\epsilon_0+\frac{4\pi i\omega}{c^2}\sigma^{\infty}(q)\right)E(q)=\left(\frac{2}{\pi}\right)^{1/2}\mathcal{E}'(+0)-\frac{4\pi i\omega}{c^2}\int_{-\infty}^{\infty}\sigma^{s}(q,-q')E(q')\,dq' , \tag{3.14}$$

where $\sigma^{\infty}(q)$ and $\sigma^{s}(q,q')$ are the Fourier transforms of $\sigma_{xx}^{\infty}(z,z')$ and $\sigma_{xx}^{s}(z,z')$, respectively. The integral in Eq. (3.14) is the Fourier transform of what we shall call the "surface current density" $j^s(z)$

$$j^s(z)=\int_{-\infty}^{\infty}\sigma_{xx}^{s}(z,z')\mathcal{E}(z')\,dz' . \tag{3.15}$$

IV. CONDUCTIVITY TENSOR OF THE UNBOUNDED MEDIUM

In this section we shall derive the conductivity due to the resonant bulk electrons. The experimental results which we want to interpret have been obtained from bisectrix plane samples, with $\vec{\mathcal{E}}$ and $\vec{H}_0$ fields both parallel to the binary axis, i.e., axis x. The cyclotron mass m_c^a of the electrons of the ellipsoid a (see Fig. 1) is almost two orders of magnitude larger than that of the electrons b and c. The same is true of the cyclotron mass of holes. The frequencies of the laser field and the values of magnetic field were such that only resonant transitions of electrons b and c could be observed. Electrons a together with holes thus contribute to the nonresonant "background" conductivity which can be described well in classical terms since, because of the large m_c, the separation between the Landau levels is very small compared to Fermi energy. However, the conductivity due to the electrons b and c which are of most interest to us here must be obtained by using quantum theory. Our derivation will be along the lines which are quite familiar.[33] It will enable us to take the nonparabolicity fully into account (within the two-band model) and also to make contact with quantities like mass shifts and lifetimes which can be, at least in principle, calculated microscopically. The incident electromagnetic field will not be quantized. We shall assume that the states of interest can be constructed of single-particle states and that the independent quasiparticle approximation is adequate. Since we assume that the two-band model is valid the one-particle states are those given by Wolff.[21] According to this model, the squared matrix elements for the spin-flipping transitions are at least two orders of magnitude smaller than those for the spin-conserving transitions [see Eq. (2.11)] and so only the later need to be taken into account.

Consistent with our assumptions, we can expand

the field operator $\psi^\dagger(\vec{x})$, using $\lambda=(\vec{k},n,s)$

$$\hat{\psi}^\dagger(\vec{x})=\sum_\lambda \psi_\lambda^\dagger(\vec{x})a_\lambda^\dagger \ , \tag{4.1}$$

where $\psi_\lambda(\vec{x})$ are the Wolff wave functions[21] and $a_\lambda^\dagger$ are the creation operators for the corresponding states. As mentioned in Sec. II, these states have characteristic degeneracy given by Eq. (2.4). The resonant part of the current operator is therefore

$$\vec{J}_{\rm op}=\tfrac{1}{2}e\sum_{\lambda,\lambda'}\int d^3x\,\{\psi_{\lambda'}^\dagger(\vec{x})\,\vec{v}_{\rm op}\psi_\lambda(\vec{x}) + \psi_\lambda(\vec{x})[\vec{v}_{\rm op}\psi_{\lambda'}(\vec{x})]^\dagger\}a_{\lambda'}^\dagger a_\lambda \ . \tag{4.2}$$

Since the spin-flipping transitions can be neglected in our case, the velocity matrix elements can be written [Eq. (2.9)]

$$\langle\psi_{\lambda'}|\vec{v}_{\rm op}|\psi_\lambda\rangle=F(E_{\lambda'},E_\lambda)\langle\chi_{\lambda'}|\vec{\alpha}^*\cdot\vec{\pi}_{\rm op}|\chi_\lambda\rangle \ . \tag{4.3}$$

The quantity $\langle\chi_{\lambda'}|\vec{\alpha}^*\cdot\vec{\pi}|\chi_\lambda\rangle$ is just the matrix element in lowest-order effective-mass theory. $\vec{\alpha}^*$ is the inverse effective-mass tensor at the bottom of the conduction band and $|\chi_\lambda\rangle$ are the eigenstates of the effective-mass Hamiltonian given by Eq. (2.10) which correspond to the set of eigenvalues $\lambda=(\vec{k},n,s)$. $\vec{\pi}_{\rm op}=\vec{p}_{\rm op}-(e/c)\vec{A}_T(\vec{x},t)$, where $\vec{A}_T(\vec{x},t)=\vec{A}_H(\vec{x})+\vec{A}(\vec{x},t)$ and $\vec{A}_H$ and $\vec{A}$ are vector potentials which belong to the applied magnetic field and incident radiation, respectively. The function $F(E_{\lambda'},E_\lambda)$ is defined to be

$$F(E_{\lambda'},E_\lambda)=\frac{1}{2}\frac{E_g(E_{\lambda'}+E_\lambda+E_g)}{[E_{\lambda'}E_\lambda(2E_{\lambda'}+E_g)(2E_\lambda+E_g)]^{1/2}} \ . \tag{4.4}$$

Making use of the substitution $\vec{\pi}_{\rm op}\rightarrow -i\hbar\vec{\nabla}-(e/c)\times[\vec{A}_H(\vec{x})+\vec{A}(\vec{x},t)]$ we rewrite the total current-density operator $\vec{J}(\vec{x},t)$ into a more convenient form

$$\vec{J}_{\rm op}(\vec{x},t)=-e\,\vec{j}_{\rm op}(\vec{x})-\frac{e^2}{c}\vec{\alpha}^*\cdot\vec{A}(\vec{x},t)\hat{n}(\vec{x}) \ , \tag{4.5}$$

where the operators $\vec{j}_{\rm op}(\vec{x})$ and $\hat{n}(\vec{x})$ are given by the following expressions:

$$\vec{j}_{\rm op}(\vec{x})\equiv\frac{\hbar}{2i}\vec{\alpha}^*\cdot\sum_{\lambda',\lambda}F(E_{\lambda'},E_\lambda)[\chi_{\lambda'}^\dagger(\vec{x})\vec{\nabla}\chi_\lambda(\vec{x})-\chi_\lambda(\vec{x})\vec{\nabla}\chi_{\lambda'}^\dagger(\vec{x})]a_{\lambda'}^\dagger a_\lambda - \frac{e^2}{c}\vec{\alpha}^*\cdot\sum_{\lambda',\lambda}F(E_{\lambda'},E_\lambda)\vec{A}_H(\vec{x})\chi_{\lambda'}^\dagger(\vec{x})\chi_\lambda(\vec{x})a_{\lambda'}^\dagger a_\lambda \ , \tag{4.6}$$

$$\hat{n}(\vec{x})\equiv\sum_{\lambda',\lambda}F(E_{\lambda'},E_\lambda)\chi_{\lambda'}^\dagger(\vec{x})\chi_\lambda(\vec{x})a_{\lambda'}^\dagger a_\lambda \ . \tag{4.7}$$

The electron current $\vec{J}(\vec{x})$ is then defined by

$$\vec{J}(\vec{x},t)=\langle\vec{J}_{\rm op}(\vec{x},t)\rangle=\vec{J}(\vec{x})e^{-i\omega t}+\text{c.c.} \tag{4.8}$$

Using the standard linear-response technique we find that

$$\vec{J}(\vec{x})=\int d^3x'\,\vec{K}^\infty(\vec{x},\vec{x}')\cdot\vec{\mathcal{E}}(\vec{x}') \ , \tag{4.9}$$

where

$$K_{ij}^\infty(\vec{x},\vec{x}')=i\frac{e^2}{\omega}\alpha_{ij}^*\langle\hat{n}(\vec{x})\rangle\delta(\vec{x}-\vec{x}')\delta_{ij} + \frac{e^2}{\hbar\omega}\int_0^\infty dt\,e^{i(\omega+i\eta)t}\times\langle[\hat{j}_i(\vec{x},t),\hat{j}_j(\vec{x}')]\rangle \tag{4.10}$$

$$(i,j=1,2,3)$$

is the conductivity kernel of the unbounded medium, due to the resonant bulk electrons.

In our geometry the induced current density and electric field are

$$\vec{\mathcal{E}}(\vec{x})=[\mathcal{E}(z),0,0], \quad \vec{j}(\vec{x})=[J(z),0,0] \ , \tag{4.11}$$

and $J(z)$ and $\mathcal{E}(z)$ are related by the one-dimensional conductivity $\sigma_R^\infty(z,z')$

$$\sigma_R^\infty(z,z')=\int dx'\,dy'\,K_{xx}^\infty(\vec{x},\vec{x}') \ , \tag{4.12}$$

where $K_{xx}^\infty(\vec{x},\vec{x}')$ is given by Eq. (4.10). The index R is used to denote the resonant part of the conductivity. The nonresonant part will be discussed later. To obtain an explicit expression for $\sigma_R^\infty(z,z')$ the eigenstates of the effective-mass Hamiltonian given by Eq. (2.10) are needed. We shall simplify the algebra by assuming that the Fermi-surface ellipsoids lie in the binary-bisectrix plane (i.e., xz plane, see Fig. 1), that is, we shall neglect the 6° tilt out of this plane. With this simplification the tensor $\vec{\alpha}_a^*$ corresponding to the ellipsoid a assumes diagonal form

$$\vec{\alpha}_a^*=\begin{pmatrix}\frac{1}{m_x^*} & 0 & 0\\ 0 & \frac{1}{m_z^*} & 0\\ 0 & 0 & \frac{1}{m_y^*}\end{pmatrix} \ . \tag{4.13}$$

(The asterisk denotes quantities at the bottom of the band.) The tensors $\vec{\alpha}^*_{b,c}$ which belong to the ellipsoids b and c, respectively, are then obtained by rotating $\vec{\alpha}^*_a$ by ± 120 about the trigonal axis

$$\vec{\alpha}^*_{b,c} = \begin{pmatrix} \alpha^*_{xx} & \mp\alpha^*_{xz} & 0 \\ \mp\alpha^*_{xz} & \alpha^*_{zz} & 0 \\ 0 & 0 & \alpha^*_{yy} \end{pmatrix}$$

$$= \frac{1}{4}\begin{pmatrix} \dfrac{1}{m_x^*}+\dfrac{3}{m_z^*} & \mp\sqrt{3}\left(\dfrac{1}{m_x^*}-\dfrac{1}{m_z^*}\right) & 0 \\ \mp\sqrt{3}\left(\dfrac{1}{m_x^*}-\dfrac{1}{m_z^*}\right) & \left(\dfrac{3}{m_x^*}+\dfrac{1}{m_z^*}\right) & 0 \\ 0 & 0 & \dfrac{4}{m_y^*} \end{pmatrix} . \tag{4.14}$$

In the Landau gauge, the magnetic field along the x axis can be described by the vector potential

$$A_x = A_z = 0, \quad A_y = -H_0 z \ . \tag{4.15}$$

Making use of the Eqs. (2.10), (4.14), and (4.15) we can write the effective-mass Hamiltonian $\hat{\mathcal{H}}^*_{b,c}$ for the electrons on the ellipsoids b and c in the form (neglecting the spin part)

$$\hat{\mathcal{H}}^*_{b,c} = \frac{1}{2}\left[\alpha^*_{xx}\hat{p}_x^2 \pm 2\alpha^*_{xz}\hat{p}_x\hat{p}_z + \alpha^*_{zz}\hat{p}_z^2 + \alpha^*_{yy}\left(\hat{p}_y + \frac{eH_0}{c}z\right)^2\right] . \tag{4.16}$$

We need to find the eigenstates of these Hamiltonians. Since $\mathcal{H}^*_{b,c}$ commute with $\hat{p}_x$ and $\hat{p}_y$ there exists a complete set of eigenstates $|E,p_x,p_y\rangle$. The Schrödinger equation then leads to the following differential equation for the z-dependent part of the wave function:

$$\frac{1}{2}\left[\alpha^*_{zz}(\hat{p}_z \mp \rho p_x)^2 + \alpha^*_{yy}\left(\frac{eH_0}{c}\right)^2 (z-z_0)^2\right]\psi(z) = \left[E - \frac{1}{2}\left(\alpha^*_{xx} - \frac{\alpha^{*2}_{xz}}{\alpha^*_{zz}}\right)p_x^2\right]\psi(z) \ , \tag{4.17}$$

where $\hat{p}_z = -i\hbar\partial/\partial z$; $\rho = \alpha^*_{xz}/\alpha^*_{zz}$; and $z_0 = -cp_y/eH_0$. The equation obtained evidently corresponds to a harmonic oscillator which is displaced both in coordinate and momentum space. The mass of the oscillator is $1/\alpha^*_{zz}$ and its frequency ω_c^*

$$\omega_c^{*2} = \alpha^*_{yy}\alpha^*_{zz}\left(\frac{eH_0}{c}\right)^2 \equiv \left(\frac{eH_0}{m_c^* c}\right)^2 . \tag{4.18}$$

Using Eq. (4.14) we find for the cyclotron mass m_c^* and the longitudinal mass m_H^*

$$m_c^* = 2\left(\frac{m_x^* m_y^* m_z^*}{3m_z^* + m_x^*}\right)^{1/2} ,$$
$$\frac{1}{m_H^*} = \alpha^*_{xx} - \frac{\alpha^{*2}_{xz}}{\alpha^*_{zz}} = \frac{4}{3m_z^* + m_x^*} , \tag{4.19}$$

in accord with the expressions (2.7). From Eq. (4.17) we infer that

$$E = (n+\tfrac{1}{2})\hbar\omega_c^* + \frac{p_x^2}{2m_H^*} . \tag{4.20}$$

The wave functions corresponding to the Hamiltonians $\mathcal{H}^*_{b,c}$ can easily be found to be ($\vec{k}_\perp \cdot \vec{k}_\perp = k_x x + k_y y$)

$$\chi_{\vec{k}ns}(\vec{x}) = e^{i\vec{k}_\perp\cdot\vec{x}_\perp} e^{\pm i\rho k_x z}\phi_{\vec{k}ns}(z) . \tag{4.21}$$

$\phi_{\vec{k}ns}(z)$ is the normalized wave function of an ordinary harmonic oscillator with its center at $z_0 = -cp_y/eH_0$

$$\phi_{\vec{k}ns}(z) = N_n e^{-(a^2/2)(z-z_0)^2} H_n[a(z-z_0)]S(s) , \tag{4.22}$$

where $a^2 = eH_0/c\hbar$ and $S(s)$ is the spin-wave function. The functions $H_n(z)$ are Hermite polynomials and N_n are the normalization constants.

From Eqs. (4.6), (4.14), and (4.21) we readily find that

$$\hat{j}_x(\vec{x}) = \frac{\hbar}{2i}\sum_{\lambda',\lambda;s'=s} \exp[i(\vec{k}_\perp - \vec{k}'_\perp)\cdot\vec{x} \pm i\rho(k_x - k'_x)z] \times\left[\frac{i(k_x+k'_x)}{m_H^*}\phi_\lambda(z)\phi_{\lambda'}(z) \mp \alpha^*_{xz}\left(\phi_{\lambda'}(z)\frac{\partial}{\partial z}\phi_\lambda(z) - \phi_\lambda(z)\frac{\partial}{\partial z}\phi_{\lambda'}(z)\right)\right] F(E_{\lambda'},E_\lambda)a^\dagger_{\lambda'}a_\lambda . \tag{4.23}$$

To calculate the current-current commutator in Eq. (4.12) we shall make the following Hartree-Fock-type approximation[32]:

$$\langle a^\dagger_{\vec{k}ms}(t)a_{\vec{k}ns}(t)a^\dagger_{\vec{k}'n's'}(0)a_{\vec{k}'m's'}(0)\rangle \simeq \langle a^\dagger_{\vec{k}ms}(t)a_{\vec{k}'m's'}(0)\rangle\langle a_{\vec{k}ns}(t)a^\dagger_{\vec{k}'n's'}(0)\rangle ,$$
$$\langle a^\dagger_{\vec{k}'n's'}(0)a_{\vec{k}'m's'}(0)a^\dagger_{\vec{k}ms}(t)a_{\vec{k}ns}(t)\rangle \simeq \langle a^\dagger_{\vec{k}'n's'}(0)a_{\vec{k}ns}(t)\rangle\langle a_{\vec{k}'m's'}(0)a^\dagger_{\vec{k}ms}(t)\rangle , \tag{4.24}$$

and further assume

$$\langle a_{\vec{k}ns}(t)a^{\dagger}_{\vec{k}'n's'}(0)\rangle \cong G^{>}_{\vec{k}ns}(t)\delta_{\vec{k}\vec{k}'}\delta_{nn'}\delta_{ss'} \ , \quad \langle a^{\dagger}_{\vec{k}'n's'}(0)a_{\vec{k}ns}(t)\rangle \cong G^{<}_{\vec{k}ns}(t)\delta_{\vec{k}\vec{k}'}\delta_{nn'}\delta_{ss'} \ , \tag{4.25}$$

where as usual $G^{\gtrless}$ has the temporal Fourier transform

$$G^{\gtrless}_{\vec{k}ns}(t)=\int\frac{d\omega}{2\pi}A_{\vec{k}ns}(\omega)\begin{bmatrix}1-f(\omega)\\ f(\omega)\end{bmatrix}e^{-i\omega t} \tag{4.26}$$

in which $f(\omega)$ is the Fermi distribution function. $A_{\vec{k}ns}(\omega)$ is the spectral distribution function. We assume that A takes the Lorentzian form with characteristic width Γ_λ [λ stands for $(\vec{k},n,s)$].

$$A_\lambda(\omega)=\frac{\Gamma_\lambda}{(\omega-E_\lambda/\hbar)^2+\Gamma_\lambda^2/4} \ . \tag{4.27}$$

If we add the contributions of electrons of ellipsoids b and c (see Fig. 1) we get

$$\int dx'\int dy'\langle[\hat{j}_x(\vec{x},t),\hat{j}_x(\vec{x}')]\rangle=\sum_{\substack{\lambda'\lambda;\vec{k}'-\vec{k}\\ s'=s}}\left(2\frac{\hbar^2k_x^2}{m_H^{*2}}\mathfrak{N}_{\lambda',\lambda}(z)\mathfrak{N}_{\lambda',\lambda}(z')+\frac{\hbar^2\alpha_{xz}^{*2}}{2}\mathfrak{M}_{\lambda',\lambda}(z)\mathfrak{M}_{\lambda',\lambda}(z')\right)F^2(E_{\lambda'},E_\lambda)$$
$$\times[G^{>}_{\lambda'}(t)G^{<}_{\lambda}(-t)-G^{<}_{\lambda'}(t)G^{>}_{\lambda}(-t)] \ , \tag{4.28}$$

where

$$\mathfrak{M}_{\lambda',\lambda}(z)\equiv\left(\phi_{\lambda'}(z)\frac{\partial}{\partial z}\phi_\lambda(z)-\phi_\lambda(z)\frac{\partial}{\partial z}\phi_{\lambda'}(z)\right) \ , \quad \mathfrak{N}_{\lambda',\lambda}(z)\equiv\phi_{\lambda'}(z)\phi_\lambda(z) \ . \tag{4.29}$$

The functions $\phi_\lambda(z)$ are given by Eq. (4.22).

We deal with the gauge current [the first term in the Eq. (4.10)] by noting that at zero frequency there is no current[33] (in the absence of Landau diamagnetism). Integration over t, together with this assumption, gives us [see Eq. (4.12)]

$$\sigma_R^{\infty}(z,z')=i\frac{e^2}{\omega}\hbar\sum_{\substack{\lambda',\lambda;\vec{k}'=\vec{k}\\ s'=s}}\int\frac{d\omega'}{2\pi}\frac{d\omega''}{2\pi}A_\lambda(\omega')A_{\lambda'}(\omega'')[f(\omega')-f(\omega'')]$$
$$\times F^2(E_{\lambda'},E_\lambda)\left(\frac{2k_x^2}{m_H^{*2}}\mathfrak{N}_{\lambda',\lambda}(z)\mathfrak{N}_{\lambda',\lambda}(z')+\frac{\alpha_{xz}^{*2}}{2}\mathfrak{M}_{\lambda',\lambda}(z)\mathfrak{M}_{\lambda',\lambda}(z')\right)$$
$$\times\left(\frac{1}{\omega-\omega''+\omega'+i\eta}-\frac{1}{\omega'-\omega''+i\eta}\right) \ . \tag{4.30}$$

Here $\lambda=(\vec{k},n,s)$. The functions $\mathfrak{N}_{\lambda',\lambda}(z)$ and $\mathfrak{M}_{\lambda',\lambda}(z)$ are given by Eq. (4.29). The evaluation of the integrals over ω' and ω'' can be carried through by contour integrations. The resulting function $\mathfrak{D}_{\lambda'\lambda}(\omega)$ can be expressed as

$$\mathfrak{D}_{\lambda'\lambda}(\omega)=\Delta_{\lambda'\lambda}(\omega)-\Delta_{\lambda'\lambda}(0) \ , \tag{4.31}$$

where $\Delta_{\lambda'\lambda}(\omega)$ is given by ($\omega_\lambda=E_\lambda/\hbar$, $\omega_{\lambda'\lambda}=\omega_{\lambda'}-\omega_\lambda$, and $\Gamma_{\lambda'\lambda}=\Gamma_{\lambda'}+\Gamma_\lambda$)

$$\Delta_{\lambda'\lambda}(\omega)=\int\frac{d\omega'}{2\pi}\frac{d\omega''}{2\pi}A_\lambda(\omega')A_{\lambda'}(\omega'')\frac{f(\omega')-f(\omega'')}{\omega-\omega''+\omega'+i\eta}$$
$$=\frac{f(\omega_\lambda+i\Gamma_\lambda/2)-f(\omega_{\lambda'}-i\Gamma_{\lambda'}/2)}{\omega-\omega_{\lambda'\lambda}+i\Gamma_{\lambda'\lambda}/2}-\frac{i}{\beta\hbar}\sum_{n=0}^{\infty}\frac{\Gamma_\lambda}{[\omega_0(n)-\omega_\lambda]^2+\Gamma_\lambda^2/4}\frac{1}{\omega_0(n)+\omega-\omega_{\lambda'}+i\Gamma_{\lambda'}/2}$$
$$+\frac{i}{\beta\hbar}\sum_{n=0}^{\infty}\frac{\Gamma_{\lambda'}}{[\omega_0(-n)-\omega_{\lambda'}]^2+\Gamma_{\lambda'}^2/4}\frac{1}{\omega_0(-n)-\omega-\omega_\lambda-i\Gamma_\lambda/2} \ . \tag{4.32}$$

$\omega_0(\pm n)$ are the complex poles of the Fermi function $f(\omega)$ and $\beta=1/kT$

$$\omega_0(\pm n)=\pm\frac{(2n+1)i\pi}{\beta\hbar}+\frac{\epsilon_F}{\hbar}, \quad n=0,1,2,3,\ldots \ . \tag{4.33}$$

It turns out that our regime ($\omega\tau \simeq 100$ and $T \sim 4.2$ K) the contribution of the poles $\omega_0(n)$ of the Fermi function [i.e., the second and third term in Eq. (4.32)] can be neglected.

Most important to us will be the Fourier transform of $\sigma_R^\infty(z,z')$ which can be written in the form $\sigma_R^\infty(q,q') = \delta(q+q')\sigma_R^\infty(q)$, where

$$\sigma_R^\infty(q) = i\frac{e^3H_0}{\omega c}\sum_{n,m,s}\int\frac{dk_x}{(2\pi)^2}\mathfrak{D}_{k_x nms}(\omega)F^2(E_{k_x ns},E_{k_x ms})\left[\frac{2k_x^2}{m_H^{*2}}\tilde{\mathfrak{N}}_{nm}(q)\tilde{\mathfrak{N}}_{nm}(-q)+\frac{\alpha_{xz}^{*2}}{2}\tilde{\mathfrak{M}}_{nm}(q)\tilde{\mathfrak{M}}_{nm}(-q)\right] . \quad (4.34)$$

The functions $\tilde{\mathfrak{N}}_{nm}(q)$ and $\tilde{\mathfrak{N}}_{nm}(q)$ are Fourier transforms of the functions $\mathfrak{N}_{nm}(z)$ and $\mathfrak{M}_{nm}(z)$, respectively [see Eqs. (4.29)]. Using a well-known formula one can readily find[34]

$$\tilde{\mathfrak{N}}_{nm}(q) = N_m N_n a^{-1}2^n\pi^{1/2}m!\,i^{n-m}\left(\frac{q}{2a}\right)^{n-m} \times \mathfrak{L}_m^{n-m}\left(\frac{q^2}{2a^2}\right)e^{-(q/2a)^2} , \quad (4.35)$$

where $n \geq m$, $a^2 = eH_0/c\hbar$, and $\mathfrak{L}_m^{n-m}(x)$ are Laguerre polynomials. N_n and N_m are the normalization constants [Eq. (4.22)]. Furthermore one finds

$$\tilde{\mathfrak{M}}_{nm}(q) = -iq\tilde{\mathfrak{N}}_{nm}(q) - 4am\tilde{\mathfrak{N}}_{nm-1}(q) + 2a^2\frac{\partial}{i\partial q}\tilde{\mathfrak{N}}_{nm}(q) . \quad (4.36)$$

V. SURFACE EFFECTS ON THE CONDUCTIVITY

Effects of the surface on the excitation of cyclotron waves have been already studied by a number of authors. (See, e.g., Ref. 1, p. 14, and work cited therein.) In particular, the experimental and theoretical work of Allen and collaborators[8] on cyclotron waves in sodium and potassium in the far-infrared shows convincingly that surface effects can be quite strong. The main results of the work already done in this area can be summarized in the conclusions that surface effects may lead to change in the amplitude of the excited wave and that they cannot much affect the character of wave propagation inside the metal.[1] This holds true particularly well when the surface reflects electrons specularly.

We pointed out already in Sec. III that in Bi at far-infrared frequencies of interest to us $R_c/\delta \simeq \frac{1}{3}$. [In the case of large quantum numbers n it is still possible to define cyclotron radius R_c similarly as in classical physics since the probability of finding an electron is strongly concentrated at the distance $R_c = \sqrt{2n+1}/a$ from the center of the "orbit" ($a^2 = eH_0/c\hbar$).] Therefore, within the distance $2R_c = 2\delta/3$ from the surface only a fraction of electrons can resonate. The rest of them strike the surface and are thus nonresonant. In the case, e.g., of spherical Fermi surfaces and classical orbits one finds that the fraction N_r/N of the resonant electrons varies with the distance from the surface as[8]

$$\frac{N_r}{N} = \begin{cases}\frac{3}{2}[(z/2R_c)-\frac{1}{3}(z/2R_c)^3], & z \leq 2R_c \\ 1, & z \geq 2R_c\end{cases} . \quad (5.1)$$

Since the field inside the sample depends strongly on the fraction of the resonating electrons[6] we cannot expect the correction term $\sigma^s(z,z')$ due to the surface effects to be negligible in our circumstances.

The expression (4.30) for the bulk conductivity $\sigma_R^\infty(z,z')$ itself suggests a possible way of determining the surface correction term. We note that $k_y = -eH_0z_0/c\hbar$, where z_0 is the center of a harmonic oscillator-type wave function and corresponds to the z coordinate of the center of a classical electron orbit. This means that when we integrate over k_y we in fact sum up the contributions of all oscillators (i.e., orbits) in the interval $[-\infty,\infty]$. Because of the collisions of electrons with the surface, there are in reality no such oscillators with centers z_0 in the region $-R_c < z_0 < R_c$. We must therefore subtract from $\sigma_R^\infty(z,z')$ the contribution $\Delta\sigma(z,z')$ of these spurious oscillators equal to [see Eqs. (4.30)–(4.32)]

$$\Delta\sigma(z,z') = i\frac{e^3H_0}{\omega c}\int_{-R_c}^{R_c}dz_0\int\frac{dk_x}{(2\pi)^2}\sum_{nms}\mathfrak{D}_{k_x nms}(\omega)F^2(E_{k_x ns},E_{k_x ms})\left[\frac{2k_x^2}{m_H^{*2}}\mathfrak{N}_{nm}(z)\mathfrak{N}_{nm}(z')+\frac{\alpha_{xz}^{*2}}{2}\mathfrak{M}_{nm}(z)\mathfrak{M}_{nm}(z')\right] . \quad (5.2)$$

This is particularly important because they are in the region closest to the surface where electric field has the largest values and because their contribution contains resonant terms.

The conductivity due to the electrons which collide with the surface depends rather strongly on the nature of surface scattering and is difficult to evaluate exactly. However, we may assume that a rough approximation to it would be good enough for our purpose since this part of the conductivity is nonresonant. If certain conditions were satisfied some of these electrons could absorb energy resonantly, due

to surface quantum states.[33] However, the relative fraction of such electrons, at a particular value of magnetic field H_0, is very small and we need not worry about their contribution. An electron close to the surface is moving periodically (assume smooth surface) in the z direction, as if acted upon by an effective potential similar to a segment of a harmonic well closed at the surface by a vertical wall.[33] The expression for the conductivity of these electrons is similar to Eq. (5.2) although their energies and wave functions are somewhat different from those of the electrons in the bulk so that, at the frequencies of interest, most of them cannot absorb energy resonantly. We may therefore assume that the conductivity of electrons which collide with the surface may be well approximated by the nonresonant part of Eq. (5.2), i.e., by the nonresonant contribution of those "orbits" which we found to be spurious because of the surface effects. It follows then that only the resonant part of Eq. (5.2) has to be subtracted from $\sigma_R^{\infty}(z,z')$ so that the surface correction term is of the form

$$\sigma^s(z,z') = -i\frac{e^3H_0}{\omega c}\int_{-R_c}^{R_c} dz_0 \int \frac{dk_x}{(2\pi)^2} \sum_{\substack{n,s \\ m=n-2}} \mathfrak{D}_{k_x nms}(\omega) F^2(E_{k_x ns}, E_{k_x ms}) \times \left[\frac{2k_x^2}{m_H^{*2}}\mathfrak{N}_{nm}(z)\mathfrak{N}_{nm}(z') + \frac{\alpha_{xz}^{*2}}{2}\mathfrak{M}_{nm}(z)\mathfrak{M}_{nm}(z')\right] . \tag{5.3}$$

VI. SURFACE IMPEDANCE—THEORY AND COMPARISON WITH EXPERIMENT

We shall not attempt to obtain the exact expression for the surface impedance, that is we shall not try to find the exact solution of the Eq. (3.14). Instead, we will make assumptions which appear to be physically sound and which greatly simplify the calculations. The resulting expressions for the surface impedance will then be confronted with the experimental results. In his paper Allen[8] discussed in detail the excitation of high-frequency ordinary cyclotron waves in a semi-infinite metal in the far-infrared. His investigations are in spirit very similar to ours, however the physical regimes are vastly different in both cases. The assumptions which we both have to make so that the problem becomes tractable therefore differ very much and the same is true for the calculations themselves. We shall see, though, that regardless of these differences some of our observations, in particular those concerning effects of the surface on the line shapes, are similar indeed.

First, we shall study the surface impedance assuming that the electric field at the resonance does not differ much from the field away from the resonance. In such circumstances we can take the variational approach, formulated by Marcus[35] and subsequently used by a number of authors dealing with the surface impedance of a metal.[7,33,36] We shall then go to the other extreme and calculate the impedance ignoring the surface scattering entirely. It will become clear that neither of these two approaches leads to a satisfactory theory of the resonance lines. They are nevertheless worth mentioning because of the insight they provide. Finally we shall calculate the surface impedance by attempting to solve the integral equation (3.14) with the effects of the surface included.

A. Variational approach

As it was already mentioned above, variational approach is useful if it can be correctly assumed that the electric field varies very little, even at the resonance, with the applied magnetic field H_0 and can be therefore well approximated by its value away from the resonance, or at $H_0=0$. Such an approach gives good results, for example, when for some reason only a small fraction of electrons can undergo resonant transitions.[7,33] In bismuth, however, this condition is not satisfied. Nevertheless one sees that the experimentally observed signal at the second harmonic is more than ten times smaller than that at the first harmonic, leading to a change in the transmitted power of only a few percent. The resonance at the second harmonic is weakened because of the retardation effects[7,8] and because the surface scattering reduces the number of the resonating electrons. It is therefore not unreasonable to expect that the variational approach should give adequate results in the cases presently considered.

The relation between electric field and current in the semi-infinite sample is given by [see Eq. (3.13)]

$$\frac{d^2}{dz^2}\mathcal{E}(z) + \epsilon_0\frac{\omega^2}{c^2}\mathcal{E}(z) = -i\frac{4\pi\omega}{c^2}j(z) . \tag{6.1}$$

If we multiply Eq. (6.1) by $\mathcal{E}(z)$ and integrate it by parts and then use the expression (3.1) for the surface impedance we get ($\mathcal{E}' \equiv d\mathcal{E}/dz$)

$$Z^{-1} = \frac{c^2}{i4\pi\omega}\mathcal{E}^{-2}(0) \times \left[-\int_0^{\infty} dz\, \mathcal{E}'^2(z) + \epsilon_0\frac{\omega^2}{c^2}\int_o^{\infty} dz\, \mathcal{E}^2(z)\right] + \int_0^{\infty} dz\, j(z)\mathcal{E}(z) . \tag{6.2}$$

Z^{-1} is stationary, for given $\mathcal{E}(0)$, at the correct electric field distribution $\mathcal{E}(z)$.[35]

Let $\sigma^0(z,z')$ be the conductivity at some value of magnetic field H_0 away from the resonance ($H_0=0$ can be chosen) and let $\mathcal{E}^0(z)$ be the corresponding electric field distribution in the sample. The surface impedance Z_0 is then determined by Eq. (6.2). If $\delta\sigma(z,z')\equiv\sigma(z,z')-\sigma^0(z,z')$ is small for all relevant values of magnetic field we may then expect the electric field $\mathcal{E}(z)$ does not differ much from $\mathcal{E}^0(z)$, even at resonance. Equation (6.2) gives then, to first order in the change in the nonlocal conductivity $\delta\sigma(z,z')$

$$Z^{-1}=Z_0^{-1}+\delta(Z^{-1}) \ , \tag{6.3}$$

where

$$\delta(Z^{-1})=\mathcal{E}^{0^{-2}}(0)\int_0^\infty dz\int_0^\infty dz'\,\mathcal{E}^0(z)\times\delta\sigma(z,z')\mathcal{E}^0(z') \ , \tag{6.4}$$

Differentiating Eq. (6.3) we find, with the same accuracy

$$\frac{\partial}{\partial H_0}Z=-Z_0^2\frac{\partial}{\partial H_0}\delta(Z^{-1}) \ . \tag{6.5}$$

Only $\sigma_R^\infty(z,z')$ varies appreciably with H_0 and thus we have to calculate the right-hand side of Eq. (6.4) with $\delta\sigma(z,z')$ replaced by $\sigma_R^\infty(z,z')$. We assume that the field $\mathcal{E}^0(z)$ has an exponential form

$$\mathcal{E}^0(z)=\mathcal{E}^0(0)e^{-z/\delta} \ , \tag{6.6}$$

where δ is a complex constant. Although this approximation is not appropriate in the anomalous skin-effect regime,[37] i.e., at microwave frequencies and low temperatures, at far-infrared frequencies we are returning to the classical skin-effect limit and the exponential approximation is more satisfactory.

To calculate $\delta(Z^{-1})$ given by Eq. (6.4) we first note that z_0 (the equivalent of the position of classical orbit center) can only have values $z_0\geq R_c$ and that the functions $\phi_n(z)$ [see Eq. (4.22)] fall to zero very rapidly when $|z-z_0|>R_c$. It is therefore a good approximation if we put

$$\int_0^\infty dz\,\phi_n(z)\phi_m(z)\simeq\int_{-\infty}^\infty dz\,\phi_n(z)\phi_m(z) \ . \tag{6.7}$$

With this approximation we can then calculate $\delta(Z^{-1})$ to obtain

$$\delta(Z^{-1})=i\delta\frac{e^3H_0}{\omega c}\sum_{n,m,s}\int\frac{dk_x}{(2\pi)^2}\mathfrak{D}_{k_x nms}(\omega)F^2(E_{k_n ns},E_{k_x ms})\,e^{-2R_c/\delta}\left[\frac{k_x^2}{m_H^{*2}}\tilde{\mathfrak{N}}_{nm}^2\left(\frac{i}{\delta}\right)+\frac{\alpha_{xz}^{*2}}{4}\tilde{\mathfrak{M}}_{nm}^2\left(\frac{i}{\delta}\right)\right] \ . \tag{6.8}$$

The functions $\mathfrak{D}$, F, $\tilde{\mathfrak{N}}$, and $\tilde{\mathfrak{M}}$ are defined by Eqs. (4.31), (4.4), (4.35), and (4.36); $R_c=\sqrt{2n+1}/a$ and $a^2=eH_0/c\hbar$. At our frequencies $\omega\tau>>1$ so that the skin effect is almost classical. If the field were the same as at $H_0=0$ we would expect δ to be real and equal to $\delta_0=c/\omega_0\simeq10^{-4}$ cm (ω_0 is plasma frequency). $(\partial/\partial H_0)Z$ was computed for a number of complex values of δ. The variationally calculated line shapes which are closest to those observed experimentally are depicted on Figs. 7(a) and 8(a). The lifetimes and the band parameters were chosen the same as for the other, more accurate calculations which will be described in the next section. They are given in Tables I and II. It should be emphasized that the results could not be improved in any essential way by changing the band parameters and the lifetimes only.

We see from the Figs. 7(a) and 8(a) that the variational approach properly accounts for some of the features of the observed spectra. Our findings are largely in agreement with the interpretation of the spectra given originally in Refs. 14 and 15 on the basis of simple considerations concerning the conditions under which the resonant transitions can occur. The second harmonic consists of two individual

TABLE I. The band parameters in bismuth assumed in our calculations of line shapes. m_c^* is the cyclotron mass at the bottom of the nonparabolic band, i.e., $m_c^*=m_c(E_F)/(1+2E_F/E_g)$. m_e is the electron mass.

f (GHz)	$m_c(E_F)/m_e$	m_c^*/m_e	E_F (meV)	E_g (meV)
890.7	0.009 44	0.001 58	29.9	12.0
964.3	0.009 32	0.001 58	29.4	12.0

TABLE II. The assumed Lorentzian widths $\hbar\Gamma_n(k_H,H_0)$ of the Landau levels at the values of k_H and H_0 at which the transition between the levels n and m occurs. All $\hbar\Gamma_n$'s are given in meV.

$f=890.7$ GHz	$f=964.3$ GHz
$\hbar\Gamma_{n=10}=0.048$	$\hbar\Gamma_{n=9}=0.063$
$\hbar\Gamma_{n=9}=0.063$	$\hbar\Gamma_{n=8}=0.026$
$\hbar\Gamma_{n\leq9}=0.107$ if $m\leq9$	$\hbar\Gamma_{n=7}=0.004$
$\hbar\Gamma_{n<9}\cong0.0$ if $m>9$	$\hbar\Gamma_{n\leq8}=0.173$ if $m\leq8$
$\hbar\Gamma_n\cong0.0$ otherwise	$\hbar\Gamma_n=0.033$ otherwise

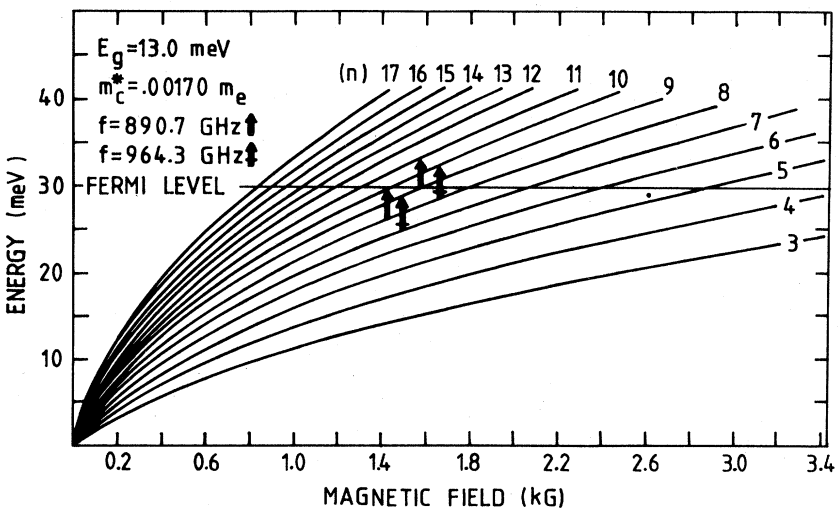

FIG. 4. Energy levels E_n ($k_H=0$) of bismuth in the nonparabolic two-band model as a function of n and magnetic field H_0. The $k_H=0$ transitions contributing the major part of the spectra are indicated by arrows. The band parameters are slightly different from those used in our calculations.

peaks, each due to distinct quantum transitions between a pair of Landau levels in the nonparabolic conduction band of bismuth. Because of the nonparabolicity, these transitions occur at different values of magnetic field. In Fig. 4 the energy levels in the Lax two-band model are depicted for $k_H=0$ and the arrows there indicate the quantum transitions which occur at that particular value of k_H. Although the calculated maxima in $\partial R/\partial H_0$ are located roughly at the magnetic field values where the $k_H=0$ transitions indicated in Fig. 4 take place,[15] the relative strength of the calculated peaks and the overall line shape (par-

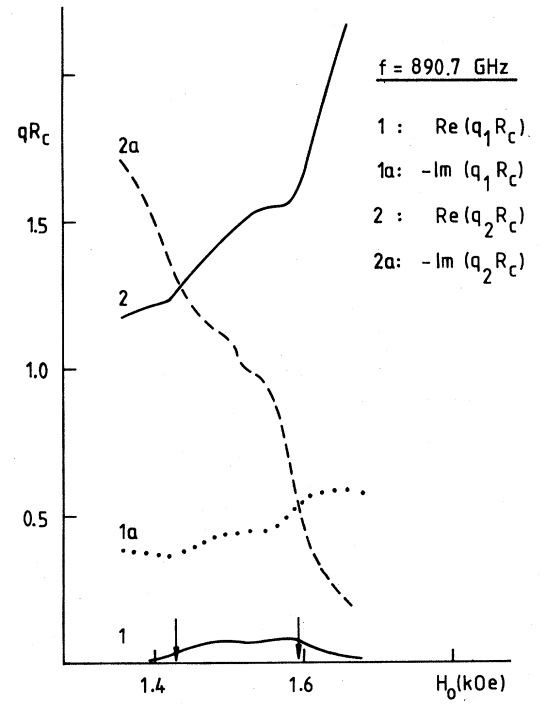

FIG. 5. Real and imaginary part of qR_c of the two cyclotron waves with the smallest wave vector q at the frequency 890.7 GHz. The positions of experimentally observed peaks at 1.427 and 1.576 kOe are marked by arrows.

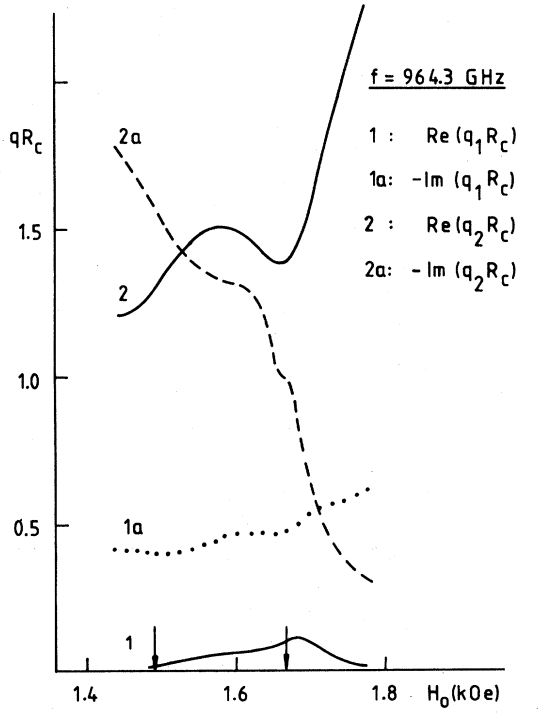

FIG. 6. Real and imaginary part of qR_c of the two cyclotron waves with the smallest wave vector q at the frequency 964.3 GHz. The positions of experimentally observed peaks at 1.485 and 1.667 kOe are marked by arrows.

ticularly on the high-field side of each peak) are substantially affected by the transitions from other values of k_H and other sets of Landau levels. These transitions can therefore generally not be neglected, contrary to the conjecture put forward in Refs. 14 and 15. This observation was confirmed by the more accurate calculations of the following section.

It is important to note [see Figs. 7(a), 7(c), 8(a), and 8(c)] that a reasonable agreement with the experimental line shapes could not be obtained with one single value of δ. Whereas the first peak in each of the two spectra could well be reproduced by a real δ, a complex value of δ must be assumed in order to reproduce the second peak. The value of δ which gives good line shape at one peak gives thus only unsatisfactory line shape at the other peak of the same spectrum. Later on we shall see that the experimentally observed spectra must indeed be attributed to two electric field modes, with their complex wave vectors q_1 and q_2 differing considerably in magnitude and in the dependence on H_0 (Figs. 5 and 6). The variational formulation of the problem is valid generally. To make practical use of it, however, we must be able to correctly assume the behavior of the electric field inside the sample. As we have seen, this behavior is rather intricate and therefore difficult to guess. The variational approach thus cannot be reliably used to study cyclotron resonance in our regime.

B. Approximate solutions to the field equation

Results of the variational calculations described in Sec. VI A show clearly that the wave effects cannot be neglected. One therefore feels inclined to go to the other extreme and ignore the effects of the surface, manifested in the conductivity $\sigma^s(z,z')$. If we neglect σ^s we get for the surface impedance [see Eqs. (3.1) and (3.14)] the expression

$$Z(H_0)=\frac{4i\omega}{c^2}\int_{-\infty}^{\infty}dq\Big/\left[-q^2+\frac{\omega^2}{c^2}\epsilon_0+\frac{4\pi i\omega}{c^2}\sigma^{\infty}(q)\right] . \tag{6.9}$$

$\sigma^{\infty}(q)$ is the Fourier transform of the total conductivity of the unbounded medium, i.e.,

$$\sigma^{\infty}(q)=\sigma_R^{\infty}(q)+\sigma_0^{\infty}(q) , \tag{6.10}$$

where $\sigma_0^{\infty}(q)$ is the nonresonant "background" conductivity of holes and electrons of the ellipsoid a (see Fig. 1). The integral in Eq. (6.9) can be, at least in principle, evaluated by contour integration. It is important to note that the wave vectors of the most relevant excitations are of the order $|q|\sim 1/\delta$, where δ is the skin depth. In our regime $R_c/\delta \ll 1$ and since $\sigma_R^{\infty}(q)$ is actually a function of y, defined by

$$y=\frac{q^2}{2a^2}=\frac{(qR_c)^2}{2(2n+1)}, \quad a^2=\frac{eH_0}{c\hbar} , \tag{6.11}$$

we may conclude that the most important contributions to the surface impedance Z come from the poles p of the integrand in Eq. (6.9) which satisfy $|p|\ll 1$. Furthermore, we may assume that in the domain $|y|\ll 1$ $\sigma^{\infty}(q)$ can be well approximated by the power-series expansion in y

$$\frac{1}{i}\sigma^{\infty}(q)\simeq s_0+s_1y+s_2y^2 . \tag{6.12}$$

The expansion for the background conductivity $\sigma_0^{\infty}(q)$ of the nonresonant electrons and holes can be obtained with the help of the formulas given by Rodriguez.[38] $\sigma_0^{\infty}(q)$ is a function of the variable $q\tau v_F/(1-i\omega\tau)\simeq iqv_F/\omega$ (since $\omega\tau\gg 1$) $|qv_F/\omega|$ is much less than 1 for the excitations $|q|\sim 1/\delta$. So for both, $\sigma_R^{\infty}(q)$ and $\sigma_0^{\infty}(q)$, the expansion around zero is needed.

The lowest two poles p_1 and p_2 of the integrand in Eq. (6.9) are then, within our approximations, equal to

$$p_1=\sqrt{y_1}, \quad p_2=\sqrt{y_2} , \tag{6.13}$$

where y_1 and y_2 are the two roots of the equation

$$y^2s_2+y\left[s_1+\frac{2a^2c^2}{4\pi\omega}\right]+s_0-\frac{\omega}{4\pi}\epsilon_0=0 . \tag{6.14}$$

The coefficients s_0, s_1, and s_2 are defined by the Eq. (6.12). For each pole p_i there is a mode of electric field with the complex wave number $q_i=\sqrt{2}ap_i$. As mentioned already, the largest part of the surface impedance Z comes from the excitations with $qR_c\ll 1$. It turns out, as we shall see later, that Z can be approximated to a sufficient degree of accuracy by the contribution of the smallest two poles. From Eqs. (6.9), (6.13), and (6.14) we then obtain, making use of the approximations introduced so far, the following expression for the surface impedance

$$Z(H_0)\simeq\frac{\sqrt{2}a}{s_2(p_1^2-p_2^2)}\left[\frac{1}{p_1}-\frac{1}{p_2}\right] . \tag{6.15}$$

In Figs. 5 and 6 the dependence of qR_c on magnetic field H_0 is depicted for the two relevant electric field modes (i.e., for the lowest two modes) with the complex wave vectors q_1 and q_2, respectively. R_c was chosen to correspond to the Landau level 9. The curves were obtained by solving the dispersion equation numerically for complex zeros, at each relevant frequency and magnetic field value. The conductivity was not approximated by the power series (6.12) for this purpose. We see that one can indeed talk of a "small-q" and a "large-q" mode, with their respective wave vectors q_1 and q_2 satisfying $|q_1R_c|\ll 1$ and $|q_2R_c|>1$. The surface impedance Z was calculated by the approximate formula (6.15) and the values of $\partial R/\partial H_0$ obtained herewith are given in Figs. 7(b) and 8(b). The dotted curves represent the

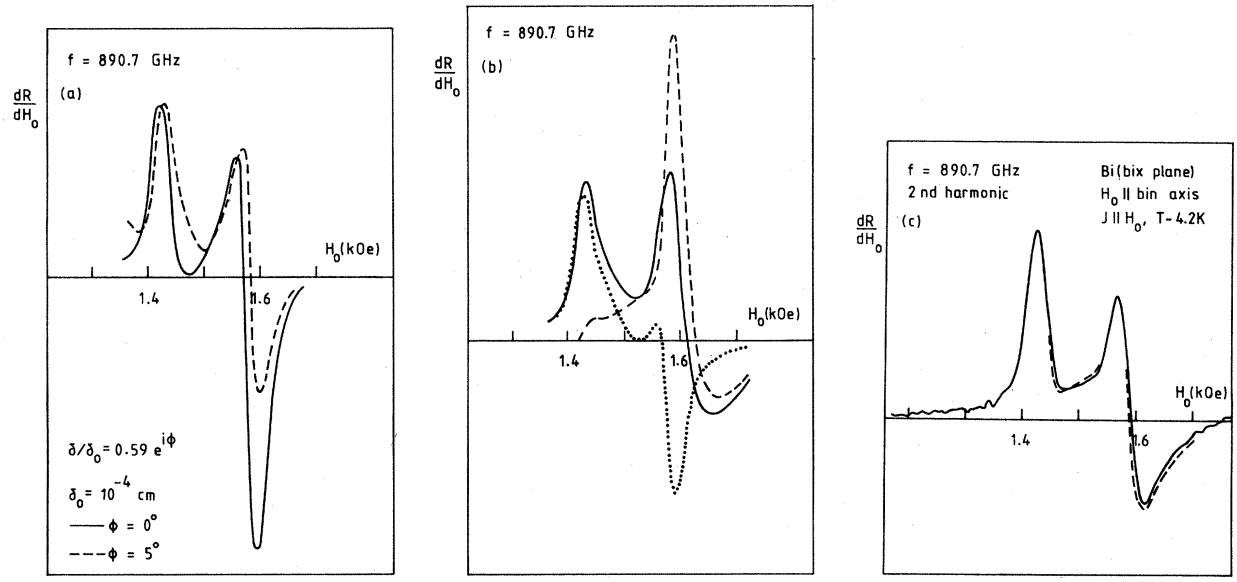

FIG. 7. (a) The variationally calculated line shapes at 890.7 GHz. Solid curve represents the result obtained by purely exponential electric field. For the broken curve the assumed field was a damped wave [see Eq. (6.6) and the δ]. (b) The line shape calculated at 890.7 GHz without surface scattering of electrons taken into account. The dotted curve represents the contribution of the small-q, the broken curve the contribution of the large-q mode. The sum of the two is represented by the solid curve. (c) The experimental line shape at 890.7 GHz (solid curve) and the corresponding result of the theory (broken curve) with the surface scattering effects included. The band parameters and lifetimes used in all calculations are given in Tables I and II.

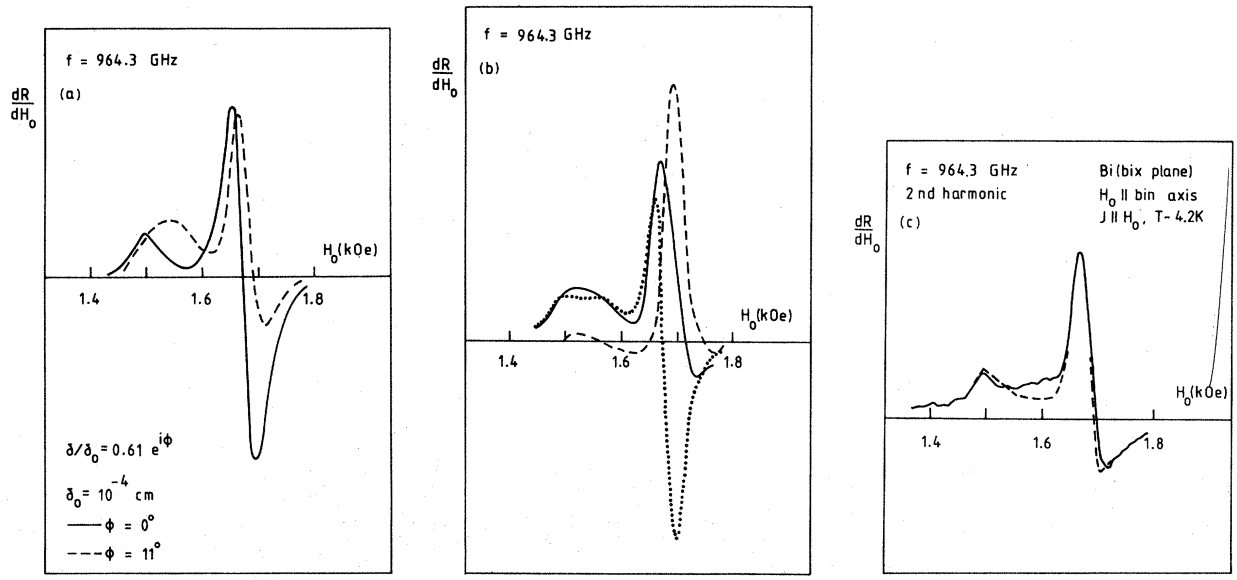

FIG. 8. (a) The variationally calculated line shapes at 964.3 GHz. Solid curve represents the result obtained by purely exponential electric field. For the broken curve the assumed field was a damped wave [see Eq. (6.6) and the δ]. (b) The line shape calculated at 964.3 GHz without surface scattering of electrons taken into account. The dotted curve represents the contribution of the small-q, the broken curve the contribution of the large-q mode. The sum of the two is represented by the solid curve. (c) The experimental line shape at 964.3 GHz (solid curve) and the corresponding result of the theory (broken curve) with the surface scattering effects included. The band parameters and lifetimes used in all calculations are given in Tables I and II.

contribution of the "small-q," and the broken curves the contribution of the "large-q" mode. Both modes together give the spectrum represented by the solid line. The calculated line shapes could be understood even better if one keeps in mind the behavior of the two modes with H_0, as illustrated by Figs. 5 and 6 (arrows there indicate the positions of the experimental peaks). We see that at the first peak the contribution of the "large-q" mode is small since the mode is strongly damped there, due to large imaginary part of q_2. The dominant electric field at the first peak is thus almost exponential in character, the real component of q_1 being very small. At higher values of H_0 the imaginary part of q_2 decreases rapidly and becomes smaller than $\mathrm{Im}(q_1)$ at the second peak where the contribution of the q_2 mode to the spectrum prevails. The variational calculations thus correctly indicated the behavior of the electric field in the sample.

Comparing Figs. 7(b), 7(c), 8(b), and 8(c) we conclude that the present approach again does not lead to satisfactory agreement with the experimental line shapes. The calculated spectra show too much absorption on the high-field side of each peak, thus indicating that damping of the waves due to surface scattering of electrons cannot be neglected. We shall have this conjecture confirmed by the more accurate calculations to be described next. It should also be pointed out that proper relative intensities of the two peaks in each spectrum could not be obtained without surface scattering being taken into account; this is particularly true in the case of the resonance at 890.7 GHz. The band parameters and lifetimes were here again chosen as given in Tables I and II, since they lead to the best agreement with the experiments in more accurate calculations. The present results, however, could not be significantly improved by solely changing the band parameters and lifetimes.

We shall now attempt to obtain in approximate solution of the field equation (3.14), with the surface scattering term included. According to the works referred to already at the beginning of Sec. V we may expect that surface scattering does not essentially change the character of the electric field inside the sample. We may therefore assume that the field is, similarly as in the preceding case (where surface effects were ignored) equal to a superposition of waves with complex wave vectors q_i and that only the two modes with the smallest magnitude of wave vector need be taken into account. Each of the modes is exponentially damped with a damping constant $1/\delta_i = \mathrm{Im}(q_i)$ which depends on H_0 in a way that may differ considerably from mode to mode (see Figs. 5 and 6). So the corresponding field could be regarded as being essentially zero outside a layer of width $\sim 2\delta_i$ around the surface. The Fourier transform $E(q)$ of the electric field is thus peaked at the values $q = \mathrm{Re}(q_i)$ and the width Δ_{q_i} of any such peak is approximately given by

$$\Delta_{q_i} \sim 2\pi/2\delta_i \ . \tag{6.16}$$

Suppose now that q is at the center of one of the peaks in $E(q)$, i.e., $q = \mathrm{Re}(q_i)$, and that Δ_{q_i} is the corresponding width of this peak. We can then write the surface term in Eq. (3.14) approximately as

$$\int_{-\infty}^{\infty} \sigma^s(q,-q')E(q')\,dq' \simeq \sigma^s(q,-q)E(q)\Delta_{q_i} + \int_{-\infty}^{\infty}{}^{\not\Delta_{q_i}} \sigma^s(q,-q')E(q')\,dq', \qquad q \simeq \mathrm{Re}(q_i) \ . \tag{6.17}$$

$\not\Delta_{q_i}$ in the second integral indicates that in the integration over q' we must exclude the region Δ_{q_i} centered at $\mathrm{Re}(q_i)$. The expression (6.17) should be a good approximation if q is near the center $\mathrm{Re}(q_i)$ of one of the peaks in $E(q)$, and may in general be less good for other values of q. This, however, may not substantially affect the results since the peak values of the Fourier transform $E(q)$ can be expected to be most important.

We now introduce an effective conductivity $\sigma_{\mathrm{eff}}(q)$, denoting by Δ_q the width of the peak of which the center is closest to q:

$$\sigma_{\mathrm{eff}}(q) \equiv \sigma^{\infty}(q) + \sigma^s(q,-q)\Delta_q \ . \tag{6.18}$$

Then the wave equation (3.14) can be approximately written as

$$\left[-q^2 + \frac{\omega^2}{c^2}\epsilon_0 + \frac{4\pi i\omega}{c^2}\sigma_{\mathrm{eff}}(q)\right]E(q) = \left[\frac{2}{\pi}\right]^{1/2} E'(+0) - \frac{4\pi i\omega}{c^2}\int_{-\infty}^{\infty}{}^{\not\Delta_q} \sigma^s(q,-q')E(q')\,dq' \ . \tag{6.19}$$

We shall, in what follows, neglect the integral in Eq. (6.19) which contains the "mode coupling" due to the surface effects. The expression for the surface impedance assumes then a form similar as in the case with no surface effects [see Eq. (6.9)], with $\sigma^{\infty}(q)$ replaced by $\sigma_{\mathrm{eff}}(q)$

$$Z(H_0) = \frac{4i\omega}{c^2}\int_{-\infty}^{\infty} dq \Big/ \left[-q^2 + \frac{\omega^2}{c^2}\epsilon_0 + \frac{4\pi i\omega}{c^2}\sigma_{\mathrm{eff}}(q)\right] \ . \tag{6.20}$$

We can then calculate the surface impedance $Z(H_0)$ assuming again that the main contribution to it comes from the two smallest poles of the integrand in Eq. (6.20) and that these poles can be calculated with sufficient accuracy by expanding $\sigma_{\mathrm{eff}}(q)$ up to

the term quadratic in $y = q^2/2a^2$, as in Eq. (6.12). These assumptions are based on the same arguments as in the calculations of $Z(H_0)$ without the surface scattering effects, earlier in this section. To carry through the calculations in the present case, we need to know Δ_q which is a function of the magnetic field H_0 and differs considerably from mode to mode (Figs. 4 and 5). For the lowest mode we may assume that, at magnetic fields well below the region where the first peak occurs, δ_1 is essentially the same as when no surface scattering is included. This should be a good approximation, since there are almost no effects of the resonance at those values of magnetic field (R_c/δ_1 is close to $\frac{1}{3}$ there, as one would expect from the usual skin effect). Furthermore, we see that, in the case of the lowest mode, δ_1 does not change much over the intervals of magnetic field of, say, 10 G, which was the separation of the points at which the derivative $\partial R/\partial H_0$ was computed. At each value of magnetic field H_0 we can then compute, together with $\partial R/\partial H_0$ also the value of δ_1 and then use this δ_1 to compute the derivative $\partial R/\partial H_0$ at the next value of magnetic field. In order to calculate the contribution of the upper mode, we first note that in this case $R_c/\delta_2 > 1$ over a large interval of magnetic field, even if surface scattering is neglected. It is clear, on physical grounds, that surface scattering should depress severely the excitation of this mode at the magnetic fields where $R_c/\delta_2 > 1$. In fact, we found it correct to assume that, for the above reasons, the excitation of the upper mode can be neglected in the region of the first peak. Somewhere between the two peaks the contribution of the upper mode is beginning to be important; it should, however, be very difficult to calculate precisely how this happens and thus to obtain correct line shape in this region. We note that at the second peak $\mathrm{Im}(q_2)$ is comparable to $\mathrm{Im}(q_1)$ and so are, of course, the corresponding δ's. On the grounds of these observations we further simplified our calculations of $Z(H_0)$, by neglecting the contribution of the upper mode over the region of the first peak, and calculating it over the remaining interval of magnetic field H_0 using the same Δ_q as for the lower mode. The results of these calculations are depicted in Figs. 7(c) and 8(c). We see that, by taking into account the effects of surface scattering, we get a much better agreement with the experiment. As expected from the discussion above, the agreement is rather poor in the region between the two peaks of the spectrum, especially at the frequency 964.3 GHz. The band parameters used in these calculations are consistent with those deduced in Ref. 15. They are given in Table I. Although the $k_H = 0$ transitions indicated in Fig. 4 were found to contribute the main part to the spectrum, transitions from other levels and other k_H values could not be neglected, contrary to the conjecture put forward in Ref. 15. To calculate the line shapes, we would thus need to know the dependence of lifetimes τ on k_H, H_0, and level number n, i.e., $\tau = \tau(n, H_0, k_H)$. This information is not available at present. It seems to be reasonable to assume that most important really are the lifetimes of the two states at the value of H_0 and k_H where the resonant transitions between these states occur. In this case it would then be sufficient to know the lifetime of each Landau level only at one particular value of H_0 and k_H. We made this rather crude approximation in our calculations of line shapes. In Table II the Lorentzian widths Γ_n which have been used here are given for each Landau level; as is well known, they are related to the lifetimes τ by $\Gamma = 1/\tau$.[39] We can say, on careful examination, that even relatively small deviations of a few percent from the Γ_n's given in Table II produce rather substantial changes in the calculated line shapes. We hope to report about a more careful study of the lifetimes in a subsequent paper.

VII. SUMMARY

Although our theory of quantum cyclotron resonance at far-infrared frequencies is not entirely rigorous, the underlying physical assumptions appear to be well justified and lead to the line shapes which agree well with the observed ones. The nonparabolic two-band model[19] seems to be adequate to study the problem. It enables us to derive the nonlocal conductivity tensor with the nonparabolicity fully taken into account. Corrections to the two-band model (Refs. 18, 30, and 31) can be included at the expense of a very complicated algebra, but otherwise without difficulties. We found that the variational approach,[35] together with the assumption that electric field in the sample has an exponential form given by Eq. (6.6), with a real δ, leads to reasonably good line shapes at the first peak of the spectra, but does not give correct line shapes at the high-field side of the second peak. Assuming then that δ is a complex (i.e., assuming that electric field in the sample is a wave) we found that the variationally calculated line shapes are improved at the second peak, but become worse at the first peak. The prevailing character of electric field in the sample thus changes from one peak to the other in a way which is difficult to predict. The variational approach, although properly accounting for some of the features of the observed spectra, is therefore not suitable for calculation of line shapes in our case [see Figs. 7(a) and 8(a)]. We continued by calculating the surface impedance of the bulk, ignoring the surface scattering altogether. As expected, the results emphasized the wave aspects rather than the resonances in quasiparticle currents [Figs. 7(b) and 8(b)] so that the calculated line shapes were again not satisfactory, showing too much absorption on the high-field side of the peaks. It

then became clear that the collisions of electrons with the surface must be taken into account. We derived corrections to the conductivity due to the effects of the surface scattering and found an approximate solution to the resulting integral equation for the Fourier transform $E(q)$ of the electric field in the sample. The properties of the electric field which can be assumed on the basis of its behavior in bulk enabled us to define an effective conductivity $\sigma_{\text{eff}}(q)$ so that the surface impedance Z, when surface scattering is present, could be approximately written in the same form as in the bulk case. The spectra thus calculated agree well with the experimental ones [Figs. 7(c) and 8(c)]. We found that the observed line shapes could be attributed to the two electric field modes with the smallest magnitude of the (complex) wave vector. The first peak in the spectrum is largely due to the lowest mode with the wave vector q_1 satisfying $\text{Im}(q_1) >> \text{Re}(q_1) \approx 0$. At the second peak the other mode, with the wave vector q_2, prevails. This mode is more "wavelike," since $\text{Re}(q_2) > \text{Im}(q_2)$. The variational calculations thus correctly indicated the behavior of the electric field.

The band parameters used in our calculations are consistent with those deduced earlier directly from the experimental results (Ref. 15). We supposed that the most important really is the relaxation rate of a Landau level at the value of k_H and the magnetic field H_0 at which the level is involved in a resonant transition. The values of these relaxation rates had to be assumed. The $k_H = 0$ transitions considered in Ref. 15 (see Fig. 4) were found to contribute the main part of the spectra. However, to obtain a satisfactory line shape (particularly on the high-field side of the resonances) transitions from other Landau levels and other k_H values had to be included in the calculations.

We mentioned already the work by Allen,[8] published on the cyclotron resonance at far-infrared frequencies in metals. Although in his case the resonance occurs in a much different regime (and, consequently, different methods must be used in calculating the line shapes) we both find that the cyclotron resonance spectra reflect considerably the excitation of cyclotron waves and that the effects of the surface scattering of electrons on these waves must be taken into account.

ACKNOWLEDGMENTS

We wish to express our gratitude to Dr. Avid Kamgar for kindly sending us her experimental curves and to the University of Maryland Computer Science Center for providing very generously the computer time for this research. One of us (A.M.) would like to thank the Center for Theoretical Physics and the Center for Materials Research of the University of Maryland, and the Research Community of Slovenia for financial support. He is furthermore much indebted to Professor S. F. Fischer for the kind hospitality at the Munich Technical University, during which parts of this work were performed, and to Professor D. Hadži of the Boris Kidrič Institute for making completion of this work possible.

---

*The main part of this work was performed when author was at the Dept. of Physics and Astronomy, University of Maryland, Md., and at the Institut für Theoretische Physik, Technische Universität München, München, Federal Republic of Germany.

†The author to whom the correspondence concerning this paper should be sent.

[1]E. A. Kaner and V. G. Skobov, *Electromagnetic Waves in Metals in a Magnetic Field* (Taylor and Francis, London, 1968).

[2]P. M. Platzman and P. A. Wolff, *Waves and Interactions in Solid State Plasmas* (Academic, New York, 1973).

[3]P. Bloomfield, Physica (Utrecht) 32, 1189 (1966).

[4]M. Ya. Azbel' and E. A. Kaner, Zh. Eksp. Teor. Fiz. 32, 896 (1957) [Sov. Phys. JETP 5, 730 (1957)]; Phys. Chem. Solids 6, 113 (1958).

[5]L. E. Hartman and J. M. Luttinger, Phys. Rev. 151, 430 (1966); E156, 1038 (1966).

[6]R. G. Chambers, Proc. Phys. Soc. London 86, 304 (1965).

[7]H. D. Drew, Phys. Rev. B 5, 360 (1972).

[8]S. J. Allen, Jr., Phys. Rev. B 9, 4121 (1974); S. J. Allen, Jr., L. W. Rupp, Jr., and P. H. Schmidt, *ibid.* 7, 5121 (1973).

[9]G. E. Smith, L. C. Hebel, and S. J. Buchsbaum, Phys. Rev. 129, 154 (1963).

[10]I. M. Lifshitz, M. Ya. Azbel', and M. I. Kaganov, Zh. Eksp. Teor. Fiz. 31, 63 (1956) [Sov. Phys. JETP 4, 41 (1957)].

[11]L. C. Hebel, Phys. Rev. 138, A1641 (1965).

[12]N. V. Brovtsyna and V. G. Skobov, Zh. Eksp. Teor. Fiz. 56, 699 (1969) [Sov. Phys. JETP 29, 379 (1969)].

[13]V. S. Edel'man, Usp. Fiz. Nauk 102, 55 (1970) [Sov. Phys. Usp. 13, 5, 583 (1971)].

[14]U. Strom, H. D. Drew, and J. F. Koch, Phys. Rev. Lett. 26, 1110 (1971).

[15]U. Strom, Avid Kamgar, and J. F. Koch, Phys. Rev. B 7, 2435 (1973).

[16]P. Goy and B. Gastaing, in *Proceedings of the Thirteenth International Conference on Low Temperature Physics*, edited by R. D.Kropschot and K. D. Timmerhaus (University of Colorado Press, Boulder, Colo., 1972).

[17]We are indebted to Dr. Avid Kamgar for this information.

[18]J. W. McClure, J. Low Temp. Phys. 25, 527 (1976).

[19]B. Lax and J. G. Mavroides, in *Advances in Solid State Physics*, edited by F. Seitz and D. Turnbull (Academic, New York, 1960), Vol. 11.

[20]M. H. Cohen and E. I. Blount, Philos. Mag. 5, 115 (1960).

[21]P. A. Wolff, J. Phys. Chem. Solids 25, 1057 (1964).

[22]M. H. Cohen, Phys. Rev. 121, 387 (1961).
[23]R. H. Bhargava, Phys. Rev. 156, 785 (1967).
[24]G. E. Smith, G. A. Baraff, and J. M. Rowell, Phys. Rev. 135, A1118 (1964).
[25]J. S. Dhillon and D. Shoenberg, Philos. Trans. R. Soc. London Ser. A 248, 1 (1955).
[26]Y. Saito, J. Phys. Soc. Jpn. 18, 1845 (1963).
[27]H. T. Chu and Y. Kao, Phys. Rev. B 1, 2369 (1970).
[28]B. McCombe and G. Seidel, Phys. Rev. 155, 633 (1966).
[29]K. Tayoda, Y. Sawada, and H. Kawamura, J. Phys. Soc. Jpn. 32, 653 (1972).
[30]G. A. Baraff, Phys. Rev. 137, A842 (1965).
[31]M. P. Vecchi, J. R. Pereira, and M. S. Dresselhaus, Phys. Rev. B 14, 298 (1976).
[32]B. Lax, K. J. Button, H. J. Zeiger, and L. M. Roth, Phys. Rev. 102, 715 (1956).
[33]R. E. Prange and T. W. Nee, Phys. Rev. 168, 779 (1968), and references mentioned therein.
[34]H. Buchholz, *Die konfluente hypergeometrische Funktion mit besonderer Berücksichtigung ihrer Anwendungen* (Springer, Berlin, 1953), p. 148.
[35]P. M. Marcus, Natl. Bur. Stand. (U.S.) Circ. No. 519, 265 (1952).
[36]M. C. Jones and E. H. Sondheimer, Proc. R. Soc. London Ser. A 278, 256 (1964).
[37]G. E. Reuter and E. H. Sondheimer, Proc. R. Soc. London Ser. A 195, 336 (1949).
[38]S. Rodriguez, Phys. Rev. 112, 84 (1958).
[39]L. P. Kadanoff and G. Baym, *Quantum Statistical Mechanics* (Benjamin, New York, 1962), p. 29.